

Type-I superconductivity in noncentrosymmetric NbGe₂

Baijiang Lv¹, Miaocong Li¹, Jia Chen¹, Yusen Yang², Siqi Wu¹, Lei Qiao¹, Feihong Guan¹, Hui Xing², Qian Tao¹, Guang-Han Cao^{1,3,5}, and Zhu-An Xu^{1,3,4,5*}

¹ Zhejiang Province Key Laboratory of Quantum Technology and Device,
Department of Physics, Zhejiang University, Hangzhou 310027, China;

² Key Laboratory of Artificial Structures and Quantum Control,
and Shanghai Center for Complex Physics, School of Physics and Astronomy,
Shanghai Jiao Tong University, Shanghai 200240, China;

³ State Key Laboratory of Silicon Materials, Zhejiang University, Hangzhou 310027, China;

⁴ Zhejiang California International NanoSystems Institute,
Zhejiang University, Hangzhou 310058, China; and

⁵ Collaborative Innovation Centre of Advanced Microstructures, Nanjing University, Nanjing 210093, China.

(Dated: August 26, 2020)

Single crystals of NbGe₂ which crystallize in a noncentrosymmetric hexagonal structure with chirality are synthesized and their superconductivity is investigated. Type-I superconductivity is confirmed by dc magnetization, field-induced second-to first-order phase transition in specific heat, and a small Ginzburg-Landau parameter $\kappa_{GL} = 0.12$. The isothermal magnetization measurements show that there is a crossover from type-I to type-II/1 superconductivity with decreasing temperature and an unusually enhanced surface superconducting critical field (H_{c3}) is discovered. The band structure calculations indicate the presence of Kramer-Weyl nodes near the Fermi level. These observations demonstrate that NbGe₂ is an interesting and rare example involving the possible interplay of type-I superconductivity, noncentrosymmetric structure and topological properties.

I. INTRODUCTION

Superconductors with noncentrosymmetric structure (NCS) have stimulated intensive research attention due to theoretically proposed possible unconventional pairing states[1][2]. In noncentrosymmetric crystal structures, the antisymmetric spin-orbit coupling (ASOC) splits the Fermi surface due to the electric field gradient in the crystal with broken inversion symmetry. Cooper pairs that originally belong to the same Fermi surface would be separated into two different Fermi surfaces. Large enough ASOC could have a significant effect on the superconducting state, leading to an admixture of spin-singlet and spin-triplet pairing states[1]. Such an admixture of pairing states usually leads to unique superconducting properties. For example, the heavy fermion superconductor CePt₃Si with a noncentrosymmetric structure has an upper critical field beyond the Pauli limit[3], and line nodes are found in the superconducting gap structure of Li₂Pt₃B[4]. Furthermore, topological superconductivity is proposed in several noncentrosymmetric compounds such as PbTaSe₂[5], BiPd[6], and YPtBi[7].

Meanwhile, according to the Ginzburg-Landau (GL) parameters κ_{GL} , superconductors can be categorized as type I with $\kappa_{GL} < 1/\sqrt{2}$, and type II with $\kappa_{GL} > 1/\sqrt{2}$. However, when κ_{GL} is close to $1/\sqrt{2}$, there will be a state between type I and type II, which is called type II/1. In the type-II/1 superconductors, magnetic flux will enter the sample, but the flux distribution will be affected by the attraction interaction between the flux lines[8]. Most superconductors belong to type II. Only a few are reported to be type I, and most of them are elementary metals with lower T_c [9]. Nevertheless, a few

binary and ternary compounds are found to be type I, for example, ScGa₃[10], Al₆Re[11], PdTe₂[12], BeAu[13], Rh₂Ga₉[14], and LiPd₂Ge[15]. Interestingly, some type-I superconductors will become type II/1 at low temperatures, accompanied by an enhanced surface superconducting state[16, 17].

Here, we report our study on the superconductivity in NbGe₂ which crystallizes in a noncentrosymmetric hexagonal structure. While the superconductivity in NbGe₂ was first discovered back in 1978[18], the interest in it has been revived since a report on a possible connection with its topological band structure in 2018[19]. In this paper, we performed systematic measurements of resistivity, magnetization and specific heat of single crystalline NbGe₂. Our study shows that it is a type-I superconductor with a crossover from type-I to type-II/1 superconductivity at low temperatures. An extremely high surface superconducting critical field (H_{c3}) is found, which implies the unconventional nature of superconductivity, possibly related to its noncentrosymmetric structure and topological properties.

II. EXPERIMENTAL DETAILS

NbGe₂ single crystals were synthesized by a two-step vapor transport technique using iodine as the transport agent. High-purity niobium (99.99%, Alfa), and germanium (99.99%, Alfa) powders were taken in a stoichiometric ratio and mixed in a glove box under argon atmosphere (the percentage of H₂O and O₂ < 0.1 ppm). The mixture was pressed into a pellet, sealed in an evacuated quartz tube and then pre-synthesized at 1073 K

for 3 days. The resultant pellet was ground into powders and mixed with 100 mg of iodine in a sealed quartz tube. Finally, the tube was placed in a two-zone furnace at 1073 K with a temperature gradient of 6 K/cm for 7 days. Single crystals with a typical shape of hexagonal pyramid were obtained after ultrasonic cleaning in ethanol.

Powder x-ray diffraction (XRD) measurements at room temperature were carried out on a PANalytical X-ray diffractometer (Model EMPYREAN) with a monochromatic $\text{CuK}\alpha_1$ radiation and a graphite monochromator. Lattice parameters were derived by Rietveld refinement using the program GSAS. The electrical resistivity and the specific heat was measured in Quantum Design physical property measurement systems (PPMS-9 and PPMS-14). A four-probe method was used for the resistivity measurements. The surface of the sample was polished before making electrical contacts, and then the gold wires were contacted to the sample by spot welding. The dc magnetization was measured on a Quantum Design magnetic property measurement system (MPMS3) equipped with a ^3He cryostat. The electronic band structure and density of states (DOS) were calculated using density functional theory employing plane-wave basis projected augmented wave (PAW) method as implemented in Vienna ab initio Simulation Package (VASP)[20, 21]. After convergence tests and full structure optimization, the lattice constants and internal atomic positions from calculation can be well compared with experimental values within 1% errorbar with an energy cut-off of 520 eV and a $15 \times 15 \times 9$ Γ -centered k -point mesh, which is sufficient to converge the total energy to 1 meV/atom.

III. RESULTS AND DISCUSSION

The XRD patterns of a NbGe_2 single crystal at room temperature are shown in Fig.1(a). Only sharp (003) and (006) peaks can be observed, which indicates a uniform c -axis orientation perpendicular to the plane of the single crystal. The inset of Fig. 1(a) shows a photograph of a typical single-crystalline sample, which naturally grows into a hexagonal pyramid shape with a typical size of $1 \times 1 \times 1 \text{ mm}^3$. The powder XRD patterns of ground NbGe_2 single crystals are displayed in Fig. 1(b). All the patterns can be well indexed with the hexagonal structure with the space group $P6_222$ (No.180). The refined lattice parameters are $a = 5.002 \text{ \AA}$, $c = 6.834 \text{ \AA}$ and $R_{wp} = 14.8\%$. The refined atomic positions are summarized in Table I. The schematic view of NbGe_2 lattice is shown in Fig. 1(c). The Ge atoms in the top and bottom layers form a honeycomb lattice, each centered by a Nb atom, and the middle two layers are alternately arranged by Nb atoms and Ge atoms. The difference between the middle two layers breaks the inversion symmetry. We

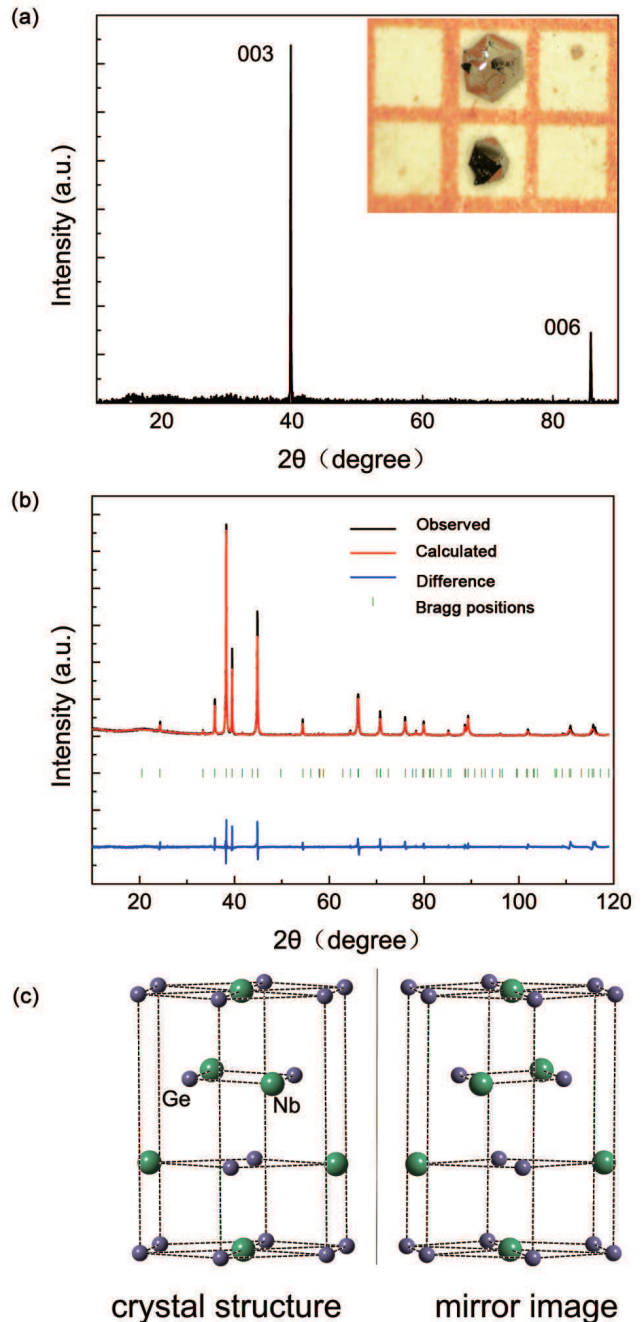


FIG. 1. (Color online) (a) XRD patterns of a NbGe_2 single crystal. The inset shows the typical single crystals used in our study. (b) Powder XRD patterns of NbGe_2 single crystals. (c) The crystal structure of NbGe_2 , which forms in the hexagonal space group $P6_222$ (No.180) with unit cell parameters 5.002 \AA and $c = 6.834 \text{ \AA}$, and its mirror image.

also note that the structure does not overlap with its mirror image, indicating that its structure is also chiral.

The dc susceptibility data measured under a magnetic field of 20 Oe ($H//c$) in both zero-field-cooled (ZFC) and field-cooled (FC) modes are shown in the Fig. 2(a). χ_{eff} has been corrected by employing the formula: $4\pi\chi_{eff} =$

TABLE I. Refined atomic positions for NbGe₂ with the space group P6₂22 (No.180) and lattice parameters $a = 5.002$ Å, $c = 6.834$ Å.

Atom	Site	X	Y	Z	Uiso
Nb	3d	0.500	0.000	0.500	0.00934
Ge	6j	0.165	0.330	0.500	0.0123

$4\pi\chi/(1 - N\chi)$, where N is the demagnetization factor and it is about 0.33 in our case[22]. Superconductivity is observed below the onset point of the diamagnetization signal, i.e., $T_c^{onset} = 2.0$ K. The superconducting volume fraction estimated from the ZFC data slightly exceeds 100%, indicating a good sample quality. Meanwhile, the relatively small difference between the ZFC and FC curves shows a very small contribution from magnetic vortices, indicating type-I superconductivity[10][11].

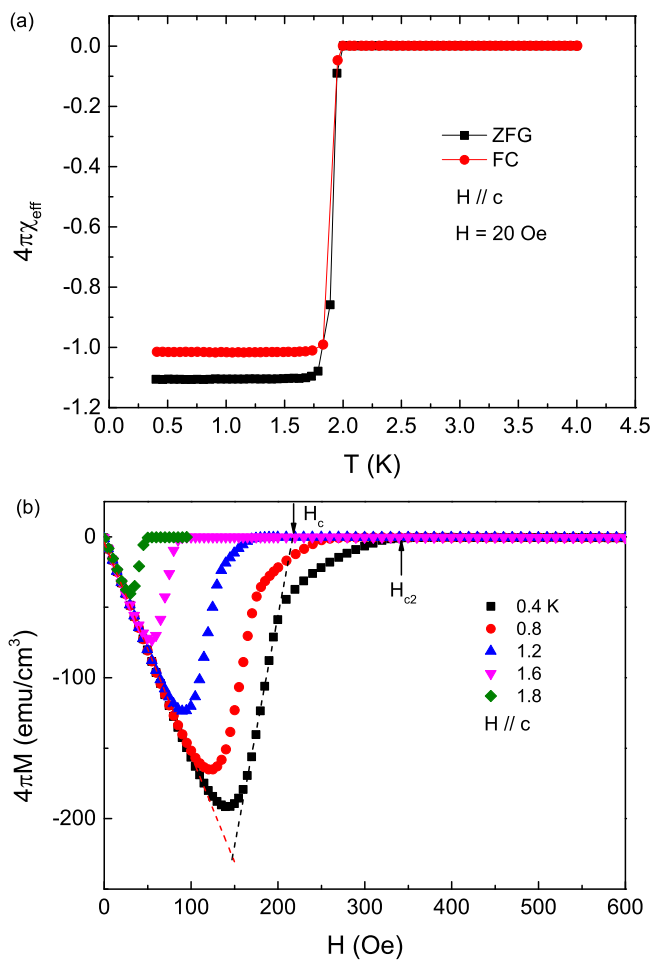


FIG. 2. (Color online) (a) Temperature dependence of the corrected dc susceptibility $\chi_{eff}(T)$ in ZFC and FC mode shows the superconductivity at $T_c^{onset} = 2.0$ K in NbGe₂. (b) Magnetization $M(H)$ curves at various temperatures.

The isothermal magnetization $4\pi M(H)$ of NbGe₂ in

the temperature range 1.8 ~ 0.4 K is displayed in Fig. 2(b). We can also get the demagnetization factor N from the initial slope $-d(4\pi M)/d(H) = 1/(1 - N)$. The obtained N value is 0.34, which is consistent with the value evaluated based on the sample shape. At higher temperatures, e.g., $T = 1.6$ and 1.8 K, the $M(H)$ curve exhibits standard type-I behavior: a sharp transition from the Meissner state to the normal state. For $T < 0.4$ K, the rounding of the $M(H)$ curves is due to the effect of the demagnetization factor[13]. We notice that in the intermediate state the $M(H)$ curve gradually deviates from linearity, and a tail appears when magnetization approaches zero. These characteristics are consistent with the reported type-II/1 superconductivity [16][17]. In the type-II/1 superconductivity, the appearance of the small tail in $M(H)$ is due to the entry of magnetic flux, which leads to a mixed state. In this case, there is a crossover from type-I to type-II/1, as temperature decreases. In the type-II/1 superconducting state, there is an attractive interaction between the flux lines[8]. As a consequence, a Meissner-mixed phase separation state, so called intermediate mixed (IM) state, is realized between the Meissner and usual mixed states[23]. Such behavior is also observed in several other type-I superconductors[16][17]. We can define H_c by extending the linear part of the curve to $M = 0$ and define H_{c2} as the point where the M reaches 0, as shown in Fig. 2(b).

Fig. 3(a) shows the temperature dependence of resistivity from 0.5 K to 300 K. The high quality of the sample is clearly demonstrated by the large ratio of room-temperature resistance to residual resistance ($RRR = \rho(300\text{ K})/\rho(2.2\text{ K})$), which is up to 970, much higher than that in earlier report (around 100)[18]. The inset of Fig. 3(a) shows the superconducting transition around $T_c^{onset} = 2.1$ K, which is consistent with the previous reports[18]. In the high temperature region ($T > 100$ K), the large room temperature resistivity and a slight negative curvature ($d^2\rho/dT^2 < 0$) was observed. Similar behavior has been observed in Nb₃Sn[24] and was interpreted using a parallel resistor model[25]. The saturation in resistivity at high temperatures usually happens when the mean free path is comparable to the inter-atomic spacing. In general, the parallel-resistor model can be written as $\frac{1}{\rho(T)} = \frac{1}{\rho_1(T)} + \frac{1}{\rho_{sat}}$, where ρ_{sat} is the temperature-independent saturation resistivity, and $\rho_1(T)$ is the ideal temperature-dependent resistivity dominated by electron-phonon scattering: $\rho_1(T) = \rho_0 + A\left(\frac{T}{\Theta_R}\right)^5 \int_0^{\frac{\Theta_R}{T}} \frac{x^5 dx}{(\exp(x)-1)(1-\exp(-x))}$, where ρ_0 denotes residual resistivity, which comes from impurities and disorder, and the second term is the generalized Bloch-Grüneisen expression. A fitting employing this model is shown in Fig. 3(a), which yields residual resistivity $\rho_0 = 0.085(0.004) \mu\Omega\text{ cm}$, $\rho_{sat} = 325.1(3) \mu\Omega\text{ cm}$, Debye temperature $\Theta_R = 335(3)$ K, $A = 490.4(4) \mu\Omega\text{ cm}$. The Debye temperature derived from the resistivity is

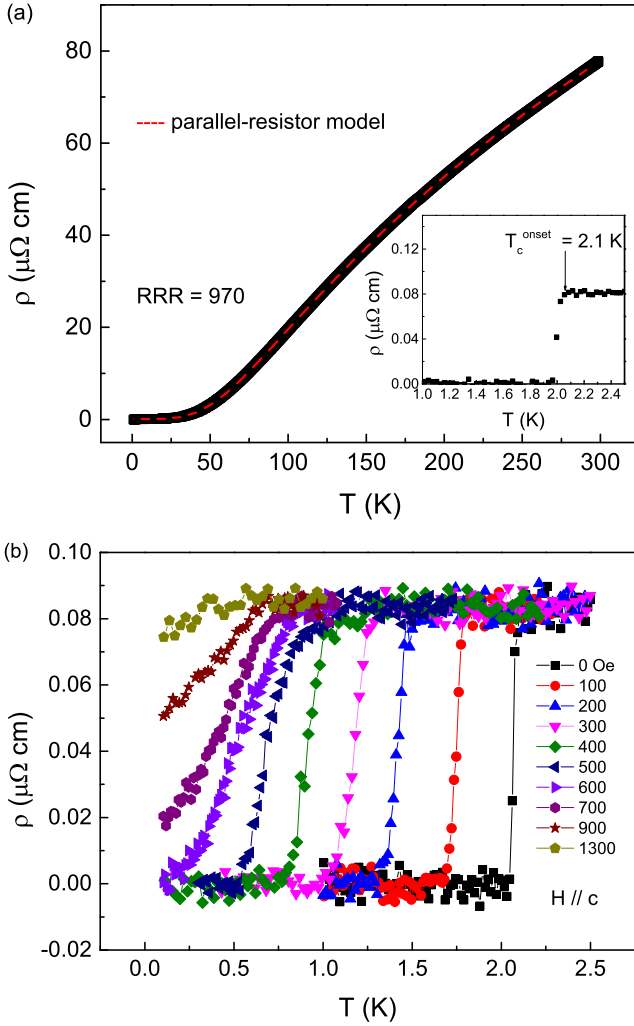


FIG. 3. (Color online) (a) Temperature dependence of the electrical resistivity. The red dashed line is a fitting curve of the parallel-resistor model. Inset is an enlarged view of the superconducting transition in NbGe₂. (b) The low-temperature resistivity (down to 0.1 K) under various magnetic fields.

comparable with that derived from the specific heat, $\Theta_D = 298$ K (see below). The saturation resistivity value is close to that reported in other compounds[24], and we can estimate the mean free path $l_{sat} = 1.27 \times 10^4 \times [\rho_{sat} \times (n^{2/3} \times S/S_F)]^{-1} = 0.2$ nm[26], which is on the same order of magnitude with inter-atomic spacing.

The low-temperature resistivity measured under various magnetic fields is shown in Fig. 3(b). The application of a magnetic field suppresses T_c rapidly, but signatures of surviving superconductivity persists up to a field of 1300 Oe, far exceeding the critical field obtained in both the magnetization and specific heat measurements. Since the resistivity is easily dominated by the surface superconducting states, the above observations may be related to the contribution from the surface superconductivity, which will be discussed in more details later.

Fig. 4(a) shows the low temperature specific heat data measured under zero field. The plot of C/T vs T^2 is shown in the inset of Fig. 4(a). A jump around $T_c = 2.0$ K, in agreement with the observations in the magnetic susceptibility and resistivity, confirms the bulk superconductivity in NbGe₂. The normal state specific-heat data above T_c consists of both electron and phonon contributions given by $C/T = \gamma_n + \beta T^2$, where γ_n is the Sommerfeld coefficient and β represents the phonon contributions. The red dashed line is the best fit to the data with $\gamma_n = 7.35$ mJ/mol K², $\beta = 0.22$ mJ/mol K⁴ (see the inset in Fig. 4(a)). The Debye model is then used with the β value in the equation $\Theta_D = (12\pi^4 NR/5\beta)^{1/3}$ to calculate the Debye temperature Θ_D , where $n = 3$ and R is the gas constant $R = 8.31$ J/mol K. The resultant Debye temperature Θ_D is 298 K. With Θ_D and T_c , the electron-phonon coupling constant λ_{ep} can then be calculated using the inverted McMillan equation[27]

$$\lambda_{ep} = \frac{1.04 + \mu^* \ln(\frac{\Theta_D}{1.45T_c})}{(1 - 0.62\mu^*) \ln(\frac{\Theta_D}{1.45T_c}) - 1.04},$$
 where μ^* is the Coulomb pseudopotential and an empirical value of 0.13 is used, and $T_c = 2$ K. It yields $\lambda_{ep} = 0.51$, suggesting this material is a weak coupling superconductor. The DOS at the Fermi level, N_{E_f} , is estimated to be 2.08 states/(eV f.u.) using the relation $N_{E_f} = \frac{3\gamma_n}{\pi^2 k_B^2 (1 + \lambda_{ep})}$.

The electronic contribution (C_{el}) to the specific heat determined by subtracting the phononic contribution from the measured specific heat data, $C_{el} = C - \beta T^3$, is shown in the main panel of Fig. 4(a). The value for the specific heat jump, $\frac{\Delta C_{el}}{\gamma_n T_c}$, was found to be 1.22, which is slightly lower than the value for a BCS isotropic gap superconductor (1.43). This indicates weakly-coupled superconductivity in NbGe₂, which is basically consistent with the value of λ_{ep} obtained above. The temperature dependence of the specific heat in the superconducting state for a single BCS gap can be obtained from the normalized entropy $S(T)$ written as: $S(T) = -\frac{6\gamma_n}{\pi^2 k_B} \int_0^\infty [f \ln f + (1-f) \ln(1-f)] d\epsilon$, where $f = (e^{\frac{E(\epsilon)}{k_B T}} + 1)^{-1}$ is the Fermi function, $E(\epsilon) = \sqrt{\epsilon^2 + \Delta^2(T)}$ is the excitation energy of quasiparticles, where ϵ is the electron energy measured relative to the chemical potential[28, 29], and $\Delta(T)$ is the temperature dependent gap function, which in the BCS s-wave model can be approximated as: $\Delta_s(T) = \Delta_0 \tanh[1.82[1.018(T_c/T - 1)]^{0.51}]$, where Δ_0 is the superconducting gap at zero temperature. The electronic specific heat is calculated by: $C_{el} = T \frac{dS}{dT}$. Fitting the specific-heat data using this model as shown by the solid red line in Fig. 4(a) yields $\alpha = \Delta_0/k_B T_c = 1.58$, which is less than the BCS value $\alpha = 1.76$ in the weak-coupling limit. Moreover, we note that the low-temperature heat capacity slightly deviates from the universal BCS s-wave model. This is likely due to the inhomogeneity of the sample which leads to the broadening of the superconducting transition[11], and another possible reason is that there may be a tiny

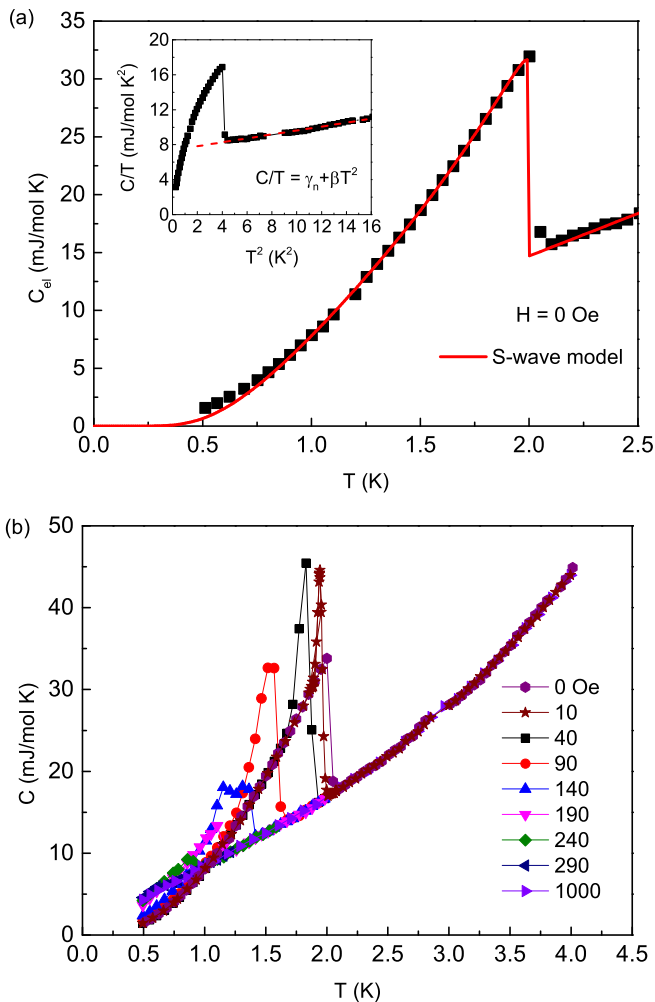


FIG. 4. (Color online) (a) Temperature dependence of electronic specific-heat and the fitting with a BCS s-wave model. Inset: C/T versus T^2 . (b) Specific heat as a function of temperature under various magnetic fields.

non-superconducting impurity phase.

Based on the Sommerfeld coefficient extracted from the specific heat data, it is possible to estimate the London penetration depth $\lambda_L(0)$, and the coherence length $\xi(0)$ [26]. Since NbGe₂ has three formula unit per unit cell, the conduction electron density n is assumed to be four electrons contributed by Nb. Thus $n = 12/V$, where V is the volume of the unit cell, and we obtain $n = 8 \times 10^{22} \text{ cm}^{-3}$. If a spherical Fermi surface ($S/S_F = 1$) is assumed for this compound, the London penetration depth is given as $\lambda_L(0) = 1.33 \times 10^8 \times \gamma^{1/2} \times (n^{2/3} S/S_F)^{-1} = 35.8 \text{ nm}$. Meanwhile, the coherence length is determined by using the BCS relation $\xi(0) = 7.95 \times 10^{-17} \times (n^{2/3} S/S_F) \times (\gamma T_c^{-1}) = 295.9 \text{ nm}$. The mean free path l_{tr} is estimated as $l_{tr} = 1.27 \times 10^4 \times [\rho_0 \times (n^{2/3} \times S/S_F)]^{-1} = 804.7 \text{ nm}$, where ρ_0 is the low-temperature normal state resistivity (0.085 $\mu\Omega \text{ cm}$ at 2.5 K). It clearly indicates that the electronic mean

free path is considerably larger than the BCS coherence length, and thus the clean limit is applied to this compound to get the GL parameter. The GL parameter $\kappa_{GL} = 0.957\lambda_L(0)/\xi(0) = 0.12$, which is obviously smaller than $\frac{1}{\sqrt{2}}$, further confirming that NbGe₂ is a type-I superconductor.

The specific heat data under magnetic fields are shown in Fig. 4(b). A sharp peak is observed under a small magnetic field of 10 Oe, which signifies a crossover from second to first-order phase transition. The similar phenomena has been observed in many type-I superconductors[10, 11], as a typical feature of type-I superconductivity. When the magnetic field gradually increases to 50 Oe, the peak magnitude also gradually increases. Upon further increasing the magnetic field, the height of the peak decreases and the peak width broadens. Far below the transition temperature, the specific heat does not change much with the magnetic field, implying negligible contributions from the magnetic vortices.

The $H - T$ phase diagram is shown in Fig. 5. H_c is determined by extrapolating the linear part of $M(H)$ curves to $M = 0$ as shown in Fig. 2(b). H_{c2} is determined by the actual zero point of $M = 0$ in the $M(H)$ curves, and also by the specific heat. The H_{c2} values from different methods are consistent with each other, as shown in Fig. 5. We also define H_{c3} as the onset point T_c^{onset} in resistivity. H_c can be well fitted by the thermodynamic critical field formula: $H(T) = H_c(0)(1 - (T/T_c)^2)$, which gives $H_c(0) = 223 \text{ Oe}$. The temperature dependence of $H_{c2}(T)$ was analyzed by means of Ginzburg-Landau (GL) model: $H(T) = H_{c2}(0) \frac{(1 - (T/T_c)^2)}{(1 + (T/T_c)^2)}$, which gives $H_{c2}(0) = 360 \text{ Oe}$. The curve of $H_{c3}(T)$ has a turning temperature T^* (shown by the arrow in Fig. 5). Below T^* , the curve shows an abnormal divergence at low temperature, and there is no sign of saturation. Meanwhile, we note that by defining T_c as the midpoint of the resistivity transition, the main features maintains (shown as blue triangle and purple cubic in the Fig. 5). T^* might be related to the crossover from type-I to type-II/1 superconductivity, similar to those found in other type-I compounds[16]. If we use linear fitting of low temperature data, we can get an roughly $H_{c3}(0)$ value equal to 2300 Oe.

In the clean limit, superconductivity is known to persist in the surface up to the surface critical field $H_{c3} \sim 1.7H_{c2}$, and it is so called standard Saint-James-de Gennes surface state[30][31]. In our case, the ratio of H_{c3}/H_{c2} equal to 6.4, much larger than 1.7. We notice that in other type-II/1 superconductors, such as the centrosymmetric ZrB₁₂, the ratio of H_{c3}/H_{c2} equals to 1.8, which is very close to the theoretical value[17]. While in another noncentrosymmetric type-II/1 superconductor LaRhSi₃, $H_{c3}/H_{c2} = 6.7$, again much larger than the theoretical value[16]. We can see that both

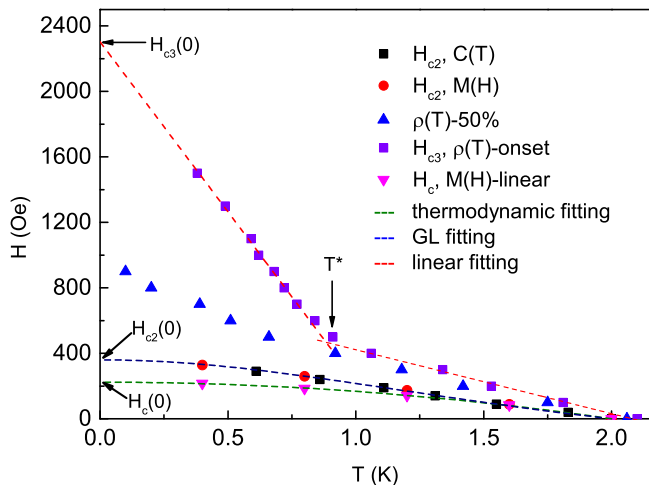


FIG. 5. (Color online) The $H - T$ phase diagram of the superconductivity of NbGe₂. H_c is estimated by extrapolating the linear part of $M(H)$ curves to $M = 0$, which is fitted by the thermodynamic critical field formula: $H(T) = H_c(0)(1 - (\frac{T}{T_c})^2)$ (green dashed line). $H_{c2}(T)$ is obtained by the actual zero point of $M = 0$ in the $M(H)$ curves, or by the specific heat, which is fitted by the GL formula: $H(T) = H_{c2}(0)\frac{(1 - (\frac{T}{T_c})^2)}{(1 + (\frac{T}{T_c})^2)}$ (blue dashed line). H_{c3} is defined as the onset point T_c^{onset} in resistivity, and $H_{c3}(0)$ is estimated by linear fitting (red dashed line).

NbGe₂ and LaRhSi₃ have an NCS structure, and this high ratio of H_{c3}/H_{c2} seems related to the NCS structure. Indeed, in the NCS structure, the ASOC leads to the surface superconductivity, which has been proposed by the theoretical studies[32][33]. There is also an alternative explanation, i.e., the existence of topological surface states may also enhance the superconducting pairing in the surface states[12][34]. For example, in the Dirac semi-metal PdTe₂, it was found that the surface superconducting critical field is much higher than the bulk[12]. It has been predicted theoretically that NbGe₂ can host Kramer-Weyl nodes near the Fermi level[19]. It is interesting to further explore whether the enhanced surface critical field is related to the topological surface states.

To further understand the properties of superconducting states of NbGe₂, density functional calculations of the electronic band structure with SOC were performed, and the results are displayed in Fig. 6(a). Near the Fermi level, the DOS is dominated by the Nb d electrons, and the value equals to 5.64 states/(eV cell) ($= 1.88$ states/(eV f.u.)), which is comparable to the experimental value estimated based on the specific heat data. We can also get the band structure value of the Sommerfeld coefficient from the density of states $\gamma_{band} = 4.4$ mJ/mol K², and the electron-phonon coupling constant λ_{ep} derived from the comparison of γ_{band} to the measured γ_n , $\lambda_{ep} = \frac{\gamma_n}{\gamma_{band}} - 1 = 0.65$, which is comparable to our previous estimated value based on the

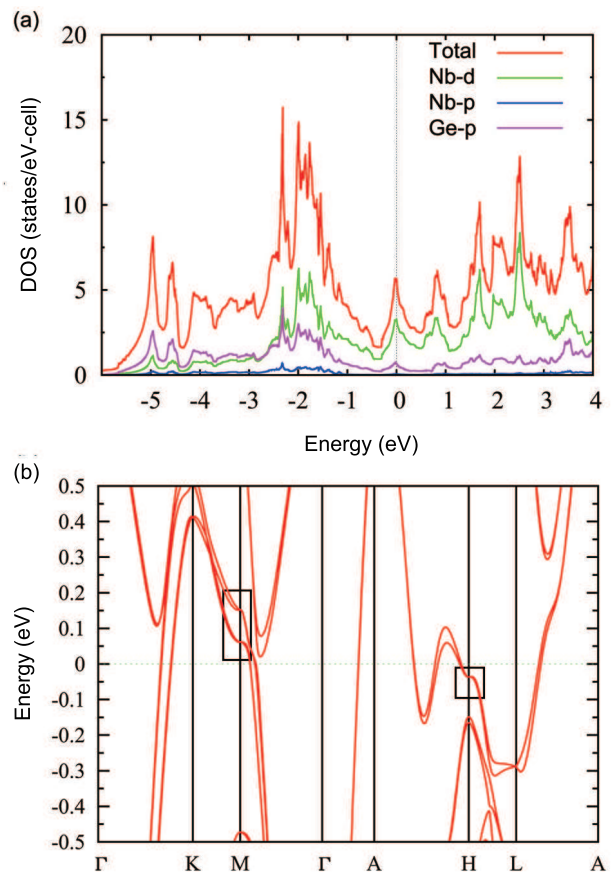


FIG. 6. (Color online) (a) The calculated DOS with SOC of NbGe₂. (b) Calculated electronic band structure within ± 0.5 eV from the Fermi energy level and Kramer-Weyl nodes denoted by the black rectangles.

McMillan equation. The finite DOS at a Fermi level also indicates the metallic ground state, supported by the electrical resistivity data. The electronic band structure calculated with (SOC) is shown in Fig. 6(b). The band splitting due to the ASOC is about ~ 40 meV, which corresponds to a moderately large ASOC effect compared to other reported NCS superconductors[1][35]. The Kramer-Weyl nodes can be found at the time reversal invariant points (shown in the black rectangle in the Fig. 6(b)), which is consistent with the previously reported band structure[19]. Some of them are very close to the Fermi level, like the nodes near the M point. Meanwhile, the superconducting state is mainly contributed by the states near the Fermi level. If these Kramer-Weyl fermions participate in the transport properties, it may have a significant effect on the superconducting state.

In order to obtain more reliable estimation of the GL parameter, we should consider the anisotropy of the Fermi velocity in the calculations[15]. The anisotropic Fermi velocity can be obtained from the band structure, and it ranges from 1.55×10^6 m/s to 6.95×10^6

m/s, hence we can get the BCS coherence length $\xi(0) \cong 0.180 \frac{\hbar v_F}{k_B T_c} \cong 1.1 \times 10^4 - 5.0 \times 10^4$ Å. London penetration depth $\lambda_L(0)$ is calculated as $\lambda_L(0) = \sqrt{\frac{3}{\mu_0 e^2 v_F^2 N_{E_f}}}$, and we obtained $\lambda_L(0) \cong 28 - 126$ Å. We determined the mean free path using the following equation [36] $l = 2.372 \times 10^{-14} \frac{m_e^*{}^2 V_M^2}{N_{E_f}^2 \rho}$, where V_M is the molar volume, ρ is low-temperature normal state resistivity, and N_{E_f} is the density of states at the Fermi level. Assuming that $\frac{m^*}{m_e} = 1$, we obtain $l = 6.74 \times 10^3$ Å, which is much smaller than the BCS coherence length $\xi(0)$, and thus the dirty limit is applied to this compound to get the GL parameter $\kappa_{GL} = 0.72 \lambda_L(0)/l(0) \cong 3.0 \times 10^{-3} - 1.3 \times 10^{-2}$. This value of GL parameter is even smaller than the value calculated based on the spherical Fermi surface, further supporting the type-I superconductivity in NbGe₂.

IV. CONCLUSION

In summary, we have synthesized NbGe₂ single crystals with high quality. Based on the resistivity, magnetization and specific heat measurements, NbGe₂ is characterized as a type-I BCS superconductor, and there is a crossover from type-I to type-II/1 superconductivity upon decreasing temperature. A surface superconducting critical field (H_{c3}) much larger than the bulk one is discovered and we propose that both the noncentrosymmetric structure and the topological state may be responsible for such behavior. NbGe₂ provides a rare example to explore the possible interplay of type-I superconductivity, noncentrosymmetric structure and topological surface states.

ACKNOWLEDGMENTS

We thank Huiqiu Yuan, Yang Liu, and Xin Lu for insightful discussions. This work was supported by the National Key R&D Program of the China (Grant No. 2016YFA0300402, and 2019YFA0308602), the National Science Foundation of China (Grant Nos. 11774305) and the Fundamental Research Funds for the Central Universities of China. DFT calculations were performed at the High Performance Computing Center of College of Science at Hangzhou Normal University.

* zhuan@zju.edu.cn

- [1] M. Smidman, M. Salamon, H. Yuan, and D. Agterberg, Rep. Prog. Phys. **80**, 036501 (2017).
 [2] E. Bauer and M. Sigrist, *Non-centrosymmetric Superconductor: Introduction and Overview* (Springer-Verlag, Heidelberg, 2012).

- [3] T. Yasuda, H. Shishido, T. Ueda, S. Hashimoto, R. Settai, T. Takeuchi, T. D Matsuda, Y. Haga, and Y. Ōnuki, J. Phys. Soc. Jpn. **73**, 1657 (2004).
 [4] H. Takeya, M. ElMassalami, S. Kasahara, and K. Hirata, Phys. Rev. B **76**, 104506 (2007).
 [5] G. Bian, T.-R. Chang, R. Sankar, S.-Y. Xu, H. Zheng, T. Neupert, C.-K. Chiu, S.-M. Huang, G. Chang, I. Belopolski, et al., Nat. Commun. **7**, 6633 (2016).
 [6] Z. Sun, M. Enayat, A. Maldonado, C. Lithgow, E. Yelland, D. C. Peets, A. Yaresko, A. P. Schnyder, and P. Wahl, Nat. Commun. **6**, (2015).
 [7] H. Kim, K. Wang, Y. Nakajima, R. Hu, S. Ziemak, P. Syers, L. Wang, H. Hodovanets, J. D. Denlinger, P. M. Brydon, et al., Sci. Adv. **4**, eaao4513 (2018).
 [8] G. Eilenberger, and H. Büttner, Z. Physik **224**, 335 (1969).
 [9] B. W. Roberts, J. Phys. Chem. Ref. Data **5**, 581 (1976).
 [10] E. Svanidze, and E. Morosan, Phys. Rev. B **85**, 174514 (2012).
 [11] D. C. Peets, E. Cheng, T. Ying, M. Kriener, X. Shen, S. Li, and D. Feng, Phys. Rev. B **99**, 144519 (2019).
 [12] H. Leng, C. Paulsen, Y. K. Huang, and A. de Visser, Phys. Rev. B **96**, 220506(R) (2017).
 [13] D. Singh, A. D. Hillier, and R. P. Singh, Phys. Rev. B **99**, 134509 (2019).
 [14] T. Shibayama, M. Nohara, H. A. Katori, Y. Okamoto, Z. Hiroi, and H. Takagi, J. Phys. Soc. Jpn. **76**, 073708 (2007).
 [15] K. Górnicka, G. Kuderowicz, E. M. Carnicom, K. Kutorasiński, B. Wiendlocha, R. J. Cava, and T. Klimczuk, Phys. Rev. B **102**, 024507 (2020).
 [16] N. Kimura, N. Kabeya, K. Saitoh, K. Satoh, H. Ogi, K. Ohsaki, and H. Aoki, J. Phys. Soc. Jpn. **85**, 024715 (2016).
 [17] Y. Wang, R. Lortz, Y. Paderno, V. Filippov, S. Abe, U. Tutsch, and A. Junod, Phys. Rev. B **72**, 024548 (2005).
 [18] J. Remeika, A. Cooper, Z. Fisk, and D. Johnston, J. Less Common Met **62**, 211 (1978).
 [19] G. Chang, B. J. Wieder, F. Schindler, D. S. Sanchez, I. Belopolski, S.-M. Huang, B. Singh, D. Wu, T.-R. Chang, T. Neupert, et al., Nat. Mater. **17**, 978 (2018).
 [20] G. Kresse, and J. Hafner, Phys. Rev. B **47**, 558 (1993).
 [21] G. Kresse, and D. Joubert, Phys. Rev. B **59**, 1758 (1999).
 [22] A. Aharoni, J. Appl. Phys. **83**, 3432 (1998).
 [23] J. Auer, and H. Ullmaier, Phys. Rev. B **7**, 136 (1973).
 [24] Z. Fisk, and G. Webb, Phys. Rev. Lett. **36**, 1084 (1976).
 [25] H. Wiesmann, M. Gurvitch, H. Lutz, A. Ghosh, B. Schwarz, M. Strongin, P. Allen, and J. Halley, Phys. Rev. Lett. **38**, 782 (1977).
 [26] T. P. Orlando, E. J. McNiff Jr, S. Foner, and M. R. Beasley, Phys. Rev. B **19**, 4545 (1979).
 [27] W. McMillan, Phys. Rev. **167**, 331 (1968).
 [28] M. Tinkham, *Introduction to Superconductivity*, 2nd ed. (Dover Publications, Mineola, NY, 1996).
 [29] H. Padamsee, J. E. Neighbor, and C. A. Shiffman, J. Low temp. Phys. **12**, 387 (1973).
 [30] D. Saint-James, and P. G. Gennes, Phys. Lett. **7**, 306 (1963).
 [31] D. Finnemore, T. Stromberg, and C. Swenson, Phys. Rev. **149**, 231 (1966).
 [32] K. Aoyama, L. Savary, and M. Sigrist, Phys. Rev. B **89**, 174518 (2014).
 [33] C. Iniotakis, S. Fujimoto, and M. Sigrist, J. Phys. Soc. Jpn. **77**, 083701 (2008).

- [34] Z. Liu, X. Yao, J. Shao, M. Zuo, L. Pi, S. Tan, C. Zhang, and Y. Zhang, *J. Am. Chem. Soc.* **137**, 10512 (2015).
- [35] Y. Nishikayama, T. Shishidou, and T. Oguchi, *J. Phys. Soc. Jpn.* **76**, 064714 (2007).
- [36] Y. Singh, C. Martin, S. L. Budko, A. Ellern, R. Prozorov, and D. C. Johnston, *Phys. Rev. B* **82**, 144532 (2010).